DNA methyltransferase inhibition restores erythropoietin production in fibrotic murine kidneys

Yu-Ting Chang,[1] Ching-Chin Yang,[1] Szu-Yu Pan,[1,2,3,4] Yu-Hsiang Chou,[1,2,4] Fan-Chi Chang,[1,2,5] Chun-Fu Lai,[2] Ming-Hsuan Tsai,[1] Huan-Lun Hsu,[2] Ching-Hung Lin,[6] Wen-Chih Chiang,[2] Ming-Shiou Wu,[2] Tzong-Shinn Chu,[2] Yung-Ming Chen,[2,4] and Shuei-Liong Lin[1,2]

[1]Graduate Institute of Physiology, College of Medicine, National Taiwan University, and [2]Renal Division, Department of Internal Medicine, National Taiwan University Hospital, Taipei, Taiwan. [3]Renal Division, Department of Internal Medicine, Far-Eastern Memorial Hospital, New Taipei, Taiwan. [4]Renal Division, Department of Internal Medicine, National Taiwan University Hospital, Yun-Lin Branch, Yun-Lin County, Taiwan. [5]Renal Division, Department of Internal Medicine, Taipei Medical University Hospital, Taipei, Taiwan. [6]Department of Oncology, National Taiwan University Hospital, Taipei, Taiwan.

Renal erythropoietin-producing cells (REPCs) remain in the kidneys of patients with chronic kidney disease, but these cells do not produce sufficient erythropoietin in response to hypoxic stimuli. Treatment with HIF stabilizers rescues erythropoietin production in these cells, but the mechanisms underlying the decreased response of REPCs in fibrotic kidneys to anemic stimulation remain elusive. Here, we show that fibroblast-like FOXD1$^+$ progenitor-derived kidney pericytes, which are characterized by the expression of α1 type I collagen and PDGFRβ, produce erythropoietin through HIF2α regulation but that production is repressed when these cells differentiate into myofibroblasts. DNA methyltransferases and erythropoietin hypermethylation are upregulated in myofibroblasts. Exposure of myofibroblasts to nanomolar concentrations of the demethylating agent 5-azacytidine increased basal expression and hypoxic induction of erythropoietin. Mechanistically, the profibrotic factor TGF-β1 induced hypermethylation and repression of erythropoietin in pericytes; these effects were prevented by 5-azacytidine treatment. These findings shed light on the molecular mechanisms underlying erythropoietin repression in kidney myofibroblasts and demonstrate that clinically relevant, nontoxic doses of 5-azacytidine can restore erythropoietin production and ameliorate anemia in the setting of kidney fibrosis in mice.

Introduction

Low levels of plasma erythropoietin (EPO) that are disproportional to the degree of anemia are often observed in patients with chronic kidney disease (CKD) (1, 2). However, the oxygen-EPO-hemoglobin feedback loop is still operating, even if at a lower set point (3). Indeed, plasma EPO concentrations in patients with CKD decline after blood transfusion and measurably increase after hemorrhage, even while levels remain low to the point of anemia (4, 5). Although hepatocytes can produce EPO in patients with CKD after hemorrhage, it is possible that renal EPO-producing cells (REPCs) continue functioning in fibrotic kidneys, but their response to anemic stimulation decreases (6). A recent clinical trial studied an inhibitor of prolyl-hydroxylase domain (PHD) enzyme, FG-2216, which stabilizes HIFs independent of oxygen availability in hemodialysis (HD) patients and healthy volunteers (7). FG-2216 increases plasma EPO levels 30.8-fold in HD patients with fibrotic kidneys, 14.5-fold in anephric HD patients, and 12.7-fold in healthy volunteers, demonstrating that enhancement of HIFs can stimulate endogenous EPO production and retain REPC function in fibrotic kidneys (7).

REPCs, which have long projections between tubules and blood vessels, are detected in the interstitium (8–13). Lineage-tracing studies have revealed that the majority of REPCs in the healthy kidney are derived from myelin protein 0–expressing (P0-expressing) cells, which are positive for CD73 (also known as ecto-5′-nucleotidase), PDGFRβ, and p75 nerve growth factor receptor and negative for PECAM-1 (also known as CD31) (11). In kidney fibrosis induced by unilateral ureteral obstruction (UUO), P0-derived cells differentiate into α smooth muscle actin (αSMA)$^+$ myofibroblasts, whose *Epo* expression decreases (11, 14). Even though various treatments can increase EPO in patients or animals with CKD (7, 11, 14), the mechanisms underlying the decreased response of myofibroblasts to the anemic stimulation remain elusive.

The regulation of *Epo* transcription is tissue specific (15, 16). While the hypoxia response element–positive (HRE$^+$) 3′-enhancer of the *Epo* gene has been confirmed to be liver specific in mice beyond embryonic day 14.5, the HRE$^+$ kidney-specific element has remained unexplored until recently (15, 16). Storti and colleagues reported that a functional HIF2α-dependent HRE in the distal 5′-enhancer is REPC specific (16). In vitro analyses have shown that methylation of the CpG islands in the promoter and 5′-untranslated region (5′-UTR) can inhibit *Epo* expression through recruiting methyl-CpG binding proteins to the promoter and hindering the binding of nuclear proteins in Hep3B human hepatoma cell line (17, 18). Moreover, methylation-free regulatory elements are a prerequisite for *Epo* expression in many human cancer cell lines (19, 20).

FOXD1$^+$ progenitors arise in the area of the neural crest and appear earlier in the same locations as P0$^+$ progenitors. FOXD1$^+$ progenitors give rise to essentially the same cells in the mature kidney as P0$^+$ progenitors (11, 21). FOXD1$^+$ progenitor-derived,

Authorship note: Y.T. Chang and C.C. Yang are co–first authors and contributed equally to this work.
Conflict of interest: The authors have declared that no conflict of interest exists.
Submitted: May 14, 2015; **Accepted:** November 16, 2015.
Reference information: *J Clin Invest*. 2016;126(2):721–731. doi:10.1172/JCI82819.

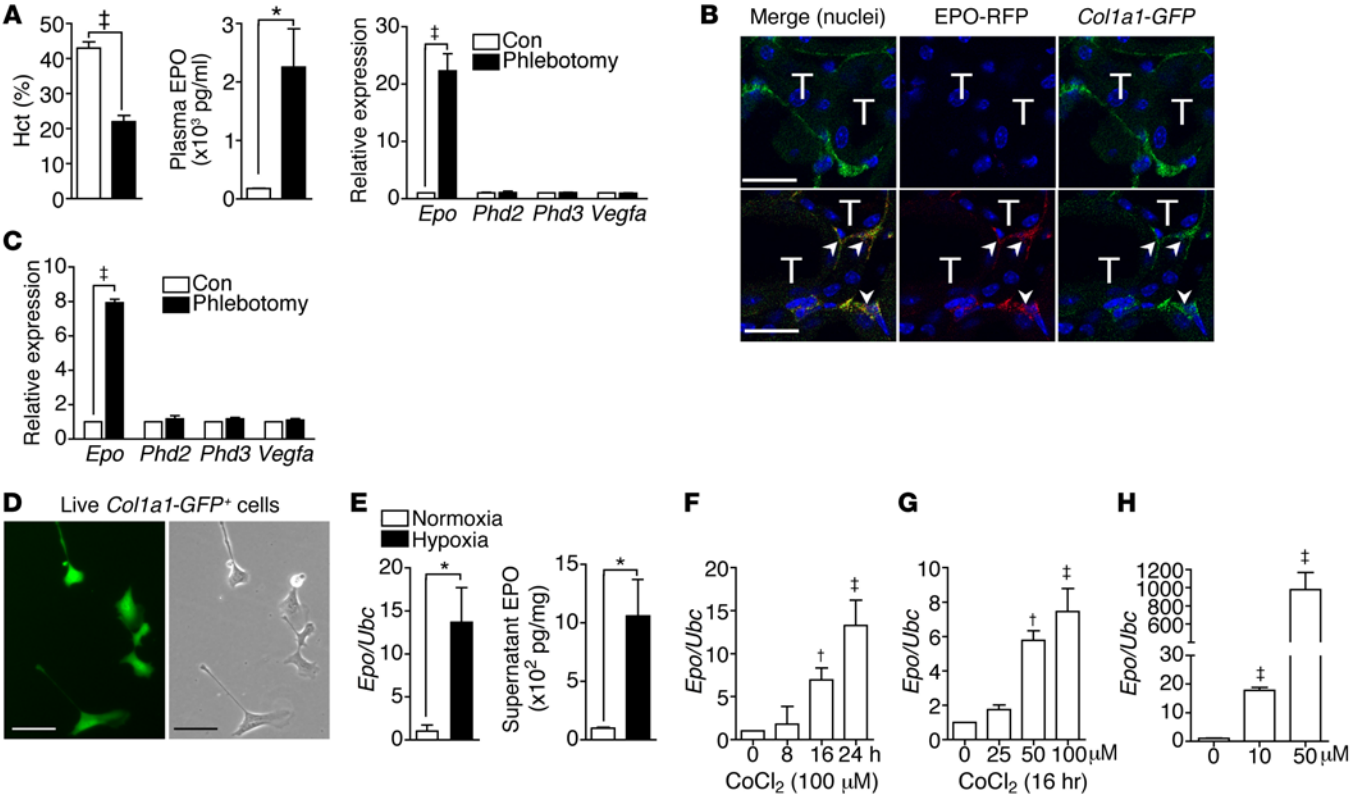

Figure 1. *Col1a1-GFP*⁺ pericytes are REPCs. (**A**) Hematocrit (Hct) and plasma EPO concentrations and renal expression of *Epo*, *Phd2*, *Phd3*, and *Vegfa* normalized by *Ubc* in mice with and without phlebotomy (Con). Phlebotomy was performed 1 day before analysis. $n = 5$ per group. (**B**) Confocal images of kidney sections of $Epo^{IRES\text{-}RFP/+}$ $Col1a1\text{-}GFP^{Tg}$ mice. Arrowheads indicate EPO-RFP⁺*Col1a1-GFP*⁺ pericytes. T, renal tubules. Original magnification, ×400. Scale bar: 20 μm. (**C**) Expression of *Epo*, *Phd2*, *Phd3*, and *Vegfa* in *Col1a1-GFP*⁺PDGFRβ⁺ kidney pericytes isolated from $Col1a1\text{-}GFP^{Tg}$ mice. $n = 5$ per group. (**D**) Fluorescent (left) and bright-field (right) images of primary cultures of live *Col1a1-GFP*⁺ kidney pericytes. Original magnification, ×400. Scale bar: 25 μm. (**E**) *Epo* expression and supernatant EPO concentration of *Col1a1-GFP*⁺ kidney pericytes cultured in chambers with normoxia (21% O_2) or hypoxia (0.5% O_2) for 24 hours. $n = 4$ per group. (**F** and **G**) *Epo* expression of *Col1a1-GFP*⁺ kidney pericytes cultured in the presence of $CoCl_2$. $n = 4$ per group. (**H**) *Epo* expression of *Col1a1-GFP*⁺ kidney pericytes cultured in the presence of IOX2 for 24 hours. $n = 4$ per group. Student's *t* test and 1-way ANOVA were used for analyses of data in **A**, **C**, and **E** and **F**–**H**, respectively. $^*P < 0.05$, $^\dagger P < 0.01$, $^\ddagger P < 0.001$.

Col1a1-GFP⁺PDGFRβ⁺ pericytes are perivascular collagen-producing cells that surround the endothelia of capillaries. These pericytes deserve attention due to their potential to produce EPO in healthy kidneys, and, as these cells stand at the junction between the circulation and the kidney, they are primed to sense the change of oxygenation and hemoglobin concentration (21–27). During fibrogenic injury, the pericytes proliferate and differentiate into myofibroblasts that produce pathogenic extracellular collagenous matrix, which leads to kidney fibrosis and function failure (22–31). In accordance with previous studies that refer to REPCs as fibroblast-like cells that might transit to myofibroblasts and contribute to kidney fibrosis (10, 11, 14), FOXD1⁺ progenitor-derived, *Col1a1-GFP*⁺PDGFRβ⁺ pericytes might provide a good model for studying the molecular mechanisms underlying the regulation of EPO expression in healthy and fibrotic kidneys. Moreover, TGF-β1, a well-recognized cytokine inducing pericyte-myofibroblast transition (29, 30), can induce *Rasal1* methylation through DNA methyltransferase 1 (DNMT1), thereby leading to perpetuation of fibroblast activation and kidney fibrosis (32). We propose that TGF-β1–induced methylation of *Epo* 5′-regulatory elements may provide a molecular basis for a decreased *Epo* response of REPCs to anemic stimulation in CKD.

Results

Kidney pericytes produce EPO. Renal *Epo* mRNA and plasma EPO concentrations were increased in mice after phlebotomy (Figure 1A). Renal expression of the other HIF-regulated genes, including prolyl-hydroxylase 2 (*Phd2*), *Phd3*, and *Vegfa*, was not changed (Figure 1A). We generated $Epo^{IRES\text{-}RFP/+}$ reporter mice by knocking *IRES-RFP* into *Epo* 3′-UTR (Supplemental Figure 1A; supplemental material available online with this article; doi:10.1172/JCI82819DS1). Renal expression of *RFP* and *Epo* increased in parallel after phlebotomy (Supplemental Figure 1B). EPO-RFP⁺ cells were detected and increased in the peritubular interstitium (Supplemental Figure 1C). Kidney pericytes were FOXD1⁺ progenitor-derived, *Col1a1-GFP*⁺, PDGFRβ⁺, CD73⁺, and p75⁺ cells (Supplemental Figure 2). We crossed $Epo^{IRES\text{-}RFP/+}$ reporter mice to $Col1a1\text{-}GFP^{Tg}$ mice to study the *Epo* expression in *Col1a1-GFP*⁺ pericytes. EPO-RFP was detectable in less than 10% of *Col1a1-GFP*⁺ pericytes in control $Epo^{IRES\text{-}RFP/+}$ $Col1a1\text{-}GFP^{Tg}$ mice; however, the percentage increased to more than 80% after phlebotomy (Figure 1B and Supplemental Figure 3, A and B). The increase of *Epo* expression was confirmed in *Col1a1-GFP*⁺ PDGFRβ⁺ pericytes isolated from kidneys of $Col1a1\text{-}GFP^{Tg}$ mice after phlebotomy (Figure 1C). We then cultured the isolated kidney pericytes in chambers containing 21% or 0.5% O_2 and confirmed

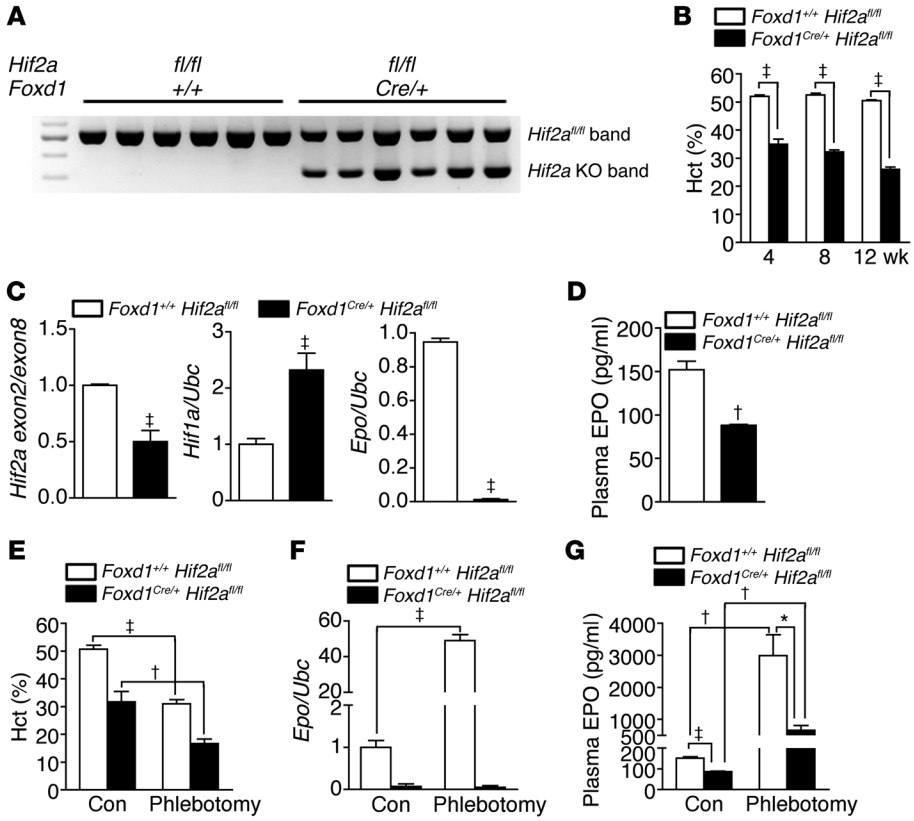

Figure 2. HIF2α regulates EPO production in kidney pericytes. (**A**) PCR products using kidney genomic DNA and genotyping primers for $Hif2a^{fl/fl}$ mice. The knockout band was confirmed in $Foxd1^{Cre/+}$ $Hif2a^{fl/fl}$ mice. $Foxd1^{+/+}$ $Hif2a^{fl/fl}$ control mice only show the $Hif2a^{fl/fl}$ band. (**B**) Analyses of hematocrit in $Foxd1^{+/+}$ $Hif2a^{fl/fl}$ and $Foxd1^{Cre/+}$ $Hif2a^{fl/fl}$ mice. n = 10 per group per time point. (**C** and **D**) Expression of renal *Hif2a*, *Hif1a*, and *Epo* and plasma EPO levels in 8-week-old adult mice. (**E**–**G**) Hematocrit, renal *Epo* expression, and plasma EPO levels in 8-week-old adult mice with and without phlebotomy. Student's t test and 1-way ANOVA were used for analyses of data in **B**–**D** and **E**–**G**, respectively. $^*P < 0.05$, $^\dagger P < 0.01$, $^\ddagger P < 0.001$.

the induction of EPO by hypoxia in pericytes (Figure 1, D and E). Cobalt chloride ($CoCl_2$), an inducer of hypoxia-like responses, increased *Epo* expression in cultured kidney pericytes (Figure 1, F and G). IOX2, a specific PHD2 inhibitor, increased EPO expression in pericytes as well (Figure 1H).

Kidney pericytes produce EPO through HIF2α regulation. To verify whether FOXD1$^+$ progenitor-derived pericytes produced EPO through HIF2α regulation that has been demonstrated in REPCs (33–35), we crossed $Foxd1^{Cre/+}$ mice with mice with a homozygous conditional *Hif2a* allele ($Hif2a^{fl/fl}$ mice) to knockout *Hif2a* in pericytes specifically. The recombination of the conditional *Hif2a* allele in $Foxd1^{Cre/+}$ $Hif2a^{fl/fl}$ mice was confirmed by PCR using kidney genomic DNA as the template (Figure 2A). Plasma levels of blood urea nitrogen (BUN) and creatinine were not different between $Foxd1^{+/+}$ $Hif2a^{fl/fl}$ control mice and $Foxd1^{Cre/+}$ $Hif2a^{fl/fl}$ knockout mice (Supplemental Figure 4). However, anemia was noted in knockout mice (Figure 2B). The knockout of *Hif2a* in *Foxd1*$^+$ progenitor-derived kidney pericytes led to a 50% decrease and 130% increase of renal *Hif2a* and *Hif1a* transcripts, respectively (Figure 2C). Compared with those in control mice, renal *Epo* transcripts and plasma EPO concentrations were reduced by 90% and 50%, respectively, in the knockout mice (Figure 2, C and D). Renal *Epo* transcripts and plasma EPO concentrations were markedly induced by phlebotomy in control mice but not in knockout mice (Figure 2, E–G). Vascular smooth muscle cells of hepatic arteries, not hepatocytes, were also *Foxd1*$^+$ progenitor derived (Supplemental Figure 5A). Hepatic *Epo* expression was increased in knockout mice, suggesting that livers took over EPO production when renal production was decreased (Figure 2, F and G, and Supplemental Figure 5B).

Transition to myofibroblasts decreases EPO expression. We then performed UUO surgery in a mouse model used to study the contralateral (CL) control and UUO fibrotic kidneys simultaneously. Phlebotomy induced robust *Epo* expression in CL kidneys but failed to do so in UUO kidneys (Figure 3, A and B). Phlebotomy did not affect *Phd3*, which had increased expression in UUO kidneys (Figure 3B). Renal *Phd2* expression was not changed by UUO injury or phlebotomy (Supplemental Figure 6). Pericytes differentiated to αSMA$^+$ myofibroblasts that retained PDGFRβ after UUO injury (Supplemental Figure 7). Analysis of pericytes and myofibroblasts isolated from CL and UUO kidneys, respectively, showed that phlebotomy-induced *Epo* expression was only noted in pericytes (Figure 3C). The expression of *Vegfa* and *Phd3*, but not *Phd2*, was higher in myofibroblasts, and expression was not changed by phlebotomy (Figure 3C). IOX2 increased *Epo* expression in cultured myofibroblasts to a much lesser degree than in pericytes (Figure 3D).

We induced the second model of kidney fibrosis by feeding mice with chow containing 0.25% adenine for 21 days (Supplemental Figure 8, A–D, and Figure 3E). Compared with that in mice fed with regular chow, renal *Epo* expression failed to increase significantly after phlebotomy in mice fed with adenine chow, although their plasma level increased to a lesser level (Figure 3, F–H). Renal expression of *Vegfa* and *Phd3* was not changed by adenine feeding and phlebotomy (Supplemental Figure 8E). Analysis of kidney pericytes and myofibroblasts isolated from mice fed with regular and adenine chow, respectively, reconfirmed that myofibroblasts failed to have a significant increase in *Epo* expression after phlebotomy (Figure 3I).

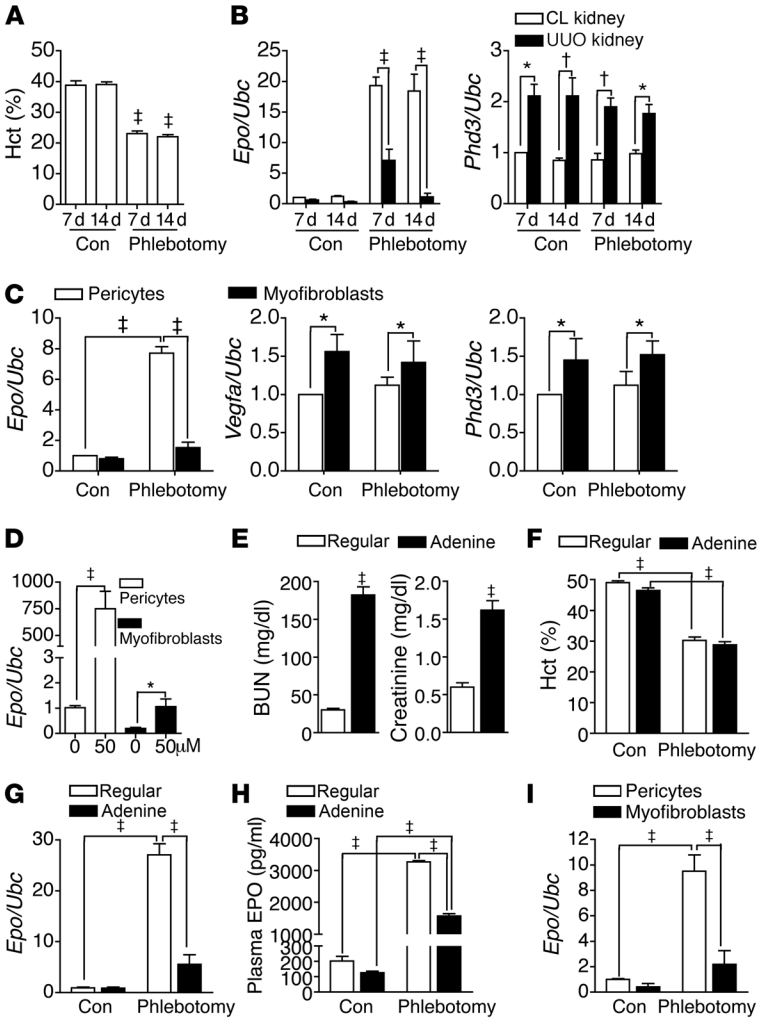

Figure 3. Myofibroblast transition represses EPO. (**A**) Hematocrit of UUO mice with or without phlebotomy 1 day before analyses at the indicated time points. *n* = 10 per group per time point. (**B**) Expression of *Epo* and *Phd3* in CL and UUO kidneys. *n* = 10 per group per time point. (**C**) Expression of *Epo*, *Vegfa*, and *Phd3* of *Col1a1-GFP*$^{+}$PDGFRβ^{+} pericytes and myofibroblasts isolated from CL kidneys and kidneys 7 days after UUO surgery from *Col1a1-GFP*^{Tg} mice, respectively. *n* = 4 per cell group. (**D**) *Epo* expression of pericytes and myofibroblasts cultured in the presence of IOX2 for 24 hours. *n* = 4 per group. (**E**) Plasma levels of BUN and creatinine in mice fed with regular chow or chow containing 0.25% adenine for 21 days. *n* = 10 per group. (**F**–**H**) Hematocrit, renal *Epo* expression, and plasma EPO levels of mice fed with regular or adenine chows. *n* = 10 per group. (**I**) *Epo* expression of *Col1a1-GFP*$^{+}$PDGFRβ^{+} pericytes and myofibroblasts isolated from kidneys of *Col1a1-GFP*^{Tg} mice fed with regular and adenine chows, respectively. *n* = 4 per cell group. One-way ANOVA was used for analyses of data in **A**–**C** and **E**–**H**, and Student's *t* test was used for analyses of data in **D**. $^{*}P < 0.05$, $^{\dagger}P < 0.01$, $^{\ddagger}P < 0.001$.

Because most mice fed with adenine chow daily did not survive after 3 weeks, we used a protocol of alternate feeding to establish a chronic model with anemia (Supplemental Figure 9A). With the elevated levels of plasma BUN and creatinine, hematocrit decreased progressively, without an increase of plasma EPO concentration in mice fed with regular and adenine chows in alternate weeks (Supplemental Figure 9, B–D). *Epo* expression decreased in kidneys but increased in livers (Supplemental Figure 9E).

Hypermethylation of Epo 5′-regulatory elements in kidney myofibroblasts. To study the mechanisms underlying the repression of *Epo* in kidney myofibroblasts, genomic DNA obtained from normal kidney pericytes and UUO kidney myofibroblasts isolated from *Col1a1-GFP*^{Tg} mice were subjected to methylation assay. Combined bisulfite restriction analysis (COBRA) showed that *Epo* promoter and 5′-UTR amplified from sodium bisulfite–converted genomic DNA of myofibroblasts was digested by restriction enzyme BstUI, suggesting the presence of hypermethylation (Figure 4, A and B). We confirmed the hypermethylation of *Epo* promoter and 5′-UTR in myofibroblasts again by bisulfite genomic sequencing (BGS) and methylation-specific PCR (MSP) (Figure 4, C–F). Hypermethylation of the distal HRE^{+} 5′-enhancer in myofibroblasts was confirmed by BGS as well (Figure 4G).

5-Azacytidine restores Epo expression in myofibroblasts and TGF-β1–exposed pericytes. To gain insights into the role of hypermethylation in *Epo* expression of myofibroblasts, we isolated and cultured kidney myofibroblasts 14 days after UUO surgery and treated these cells with 500 nM 5-azacytidine (Aza) (Figure 5A). We found that transient 3-day exposure of myofibroblasts to Aza followed by 2-day drug-free culture led to evident inhibition on DNMT1 and demethylation of *Epo* 5′-UTR (Figure 5, A–C). No cell apoptosis or change in cell cycle was noted (Figure 5, D and E). Demethylation by Aza increased not only the basal expression, but also the $CoCl_2$-induced expression of *Epo* (Figure 5, A and F). Moreover the expression of *Acta2* in myofibroblasts was decreased by Aza treatment (Figure 5G), suggesting the potential of demethylation to redifferentiate myofibroblasts back to pericytes. However, Aza did not affect the expression of *Phd3* and *Vegfa* (Figure 5F). Given that TGF-β1 is the major growth factor inducing pericyte-myofibroblast transition, we studied the effect of TGF-β1 on *Epo* expression of kidney pericytes. Cultured pericytes increased expression of *Dnmt* isoforms, notably *Dnmt1* and *Dnmt3a*, in the presence of TGF-β1 (Figure 5H). *Epo* methylation and repression in pericytes was induced by TGF-β1, which was prevented by Aza (Figure 5, I–K). By contrast, TGF-β1 increased *Vegfa* expression but did not affect *Phd3* (Figure 5K).

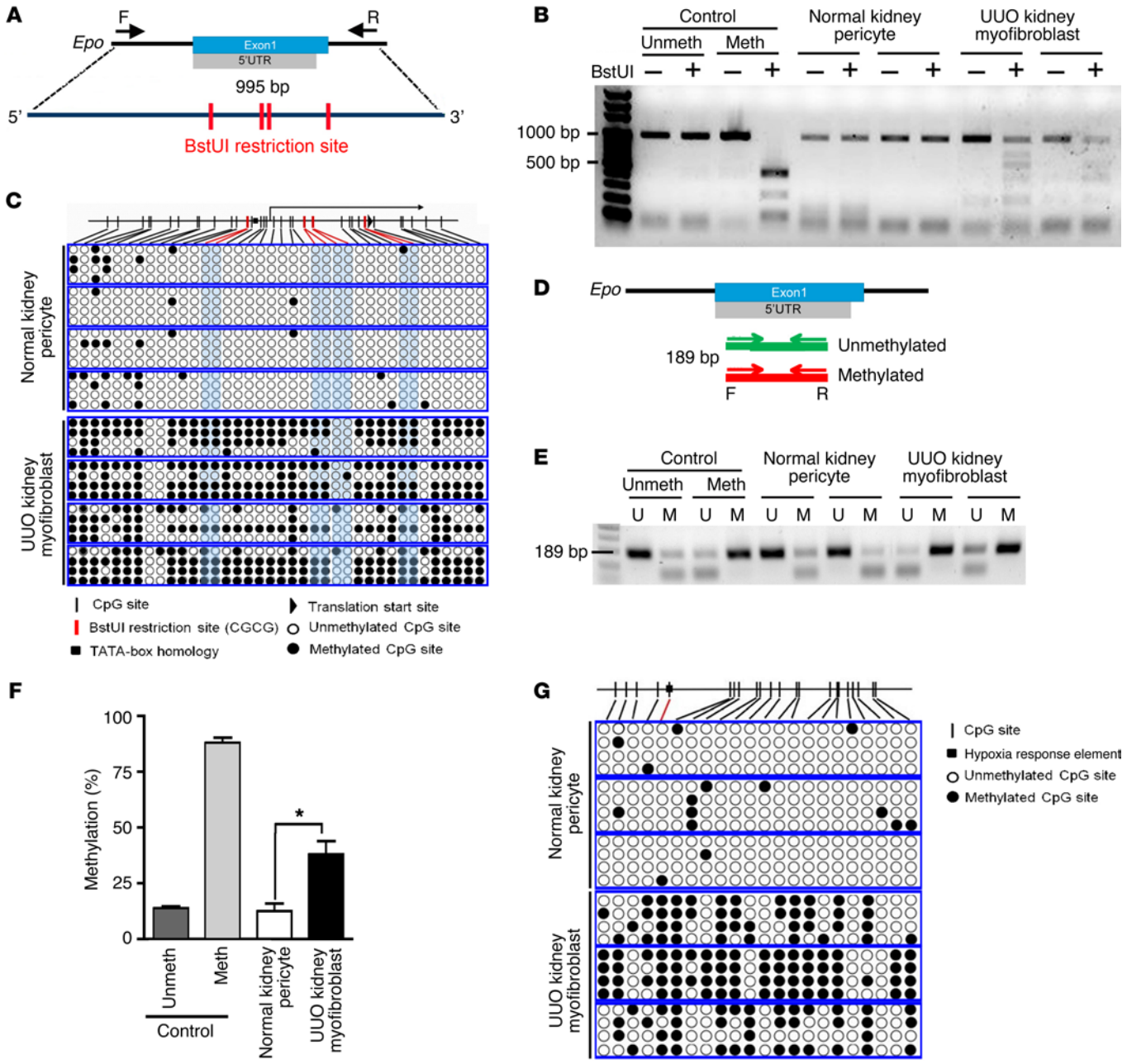

Figure 4. Hypermethylation of *EPO* 5′-regulatory elements in kidney myofibroblasts. (**A**) Schema of COBRA, illustrating the locations of PCR primers (forward and reverse for amplifying bisulfite-converted genomic DNA and recognition sites of the BstUI restriction enzyme in the *Epo* promoter and 5′-UTR. (**B**) Representative COBRA showing the electrophoresis of PCR products with (+) or without (–) BstUI digestion from 3 independent experiments. Bisulfite-converted genomic DNA was prepared from pericytes and myofibroblasts isolated from normal kidneys and kidneys 14 days after UUO surgery from *Col1a1-GFP*^{Tg} mice, respectively. Meth, methylated; Unmeth, unmethylated controls. (**C**) BGS of *Epo* promoter and 5′-UTR of pericytes and myofibroblasts. Each box represents the bisulfite genomic sequence of the indicated cell isolated from one *Col1a1-GFP*^{Tg} mouse; each row represents a single sequenced clone (4 clones from each mouse); and each dot represents a single CpG. (**D**) Schema of MSP illustrating the locations of primers for unmethylated and methylated *Epo* 5′-UTR. (**E**) Representative electrophoresis of MSP using primers for unmethylated (U) and methylated (M) *Epo* 5′-UTR. (**F**) The percentage of *Epo* 5′-UTR methylation in pericytes and myofibroblasts determined by the densitometric analyses of MSP products. $n = 4$ per cell group. (**G**) BGS of *Epo* distal HRE$^+$ 5′-enhancer of pericytes and myofibroblasts. Boxes, rows, and dots are as defined in the legend for **C**. The sequences of PCR primers are shown in Supplemental Table 2. One-way ANOVA was used for analyses of data in **A**–**C** and **E**–**H**, and Student's *t* test was used for analyses of data in **D**. $^*P < 0.05$.

Aza restores EPO expression and ameliorates anemia in mouse models of kidney fibrosis. We then confirmed the expression of *Dnmt* isoforms by quantitative PCR in mouse models of kidney fibrosis induced by UUO and adenine (Figure 6A and Supplemental Figure 8F). Confocal microscopy detected DNMT1 in kidney myofibroblasts of *Col1a1-GFP*^{Tg} mice (Figure 6B). DNMT3a, not DNMT3b, was expressed in both pericytes and myofibroblasts (Figure 6B). Because the UUO mouse model, which showed normal hematocrit and plasma levels of BUN and creatinine, could be used to study the CL control and UUO fibrotic kidneys simultaneously, we first

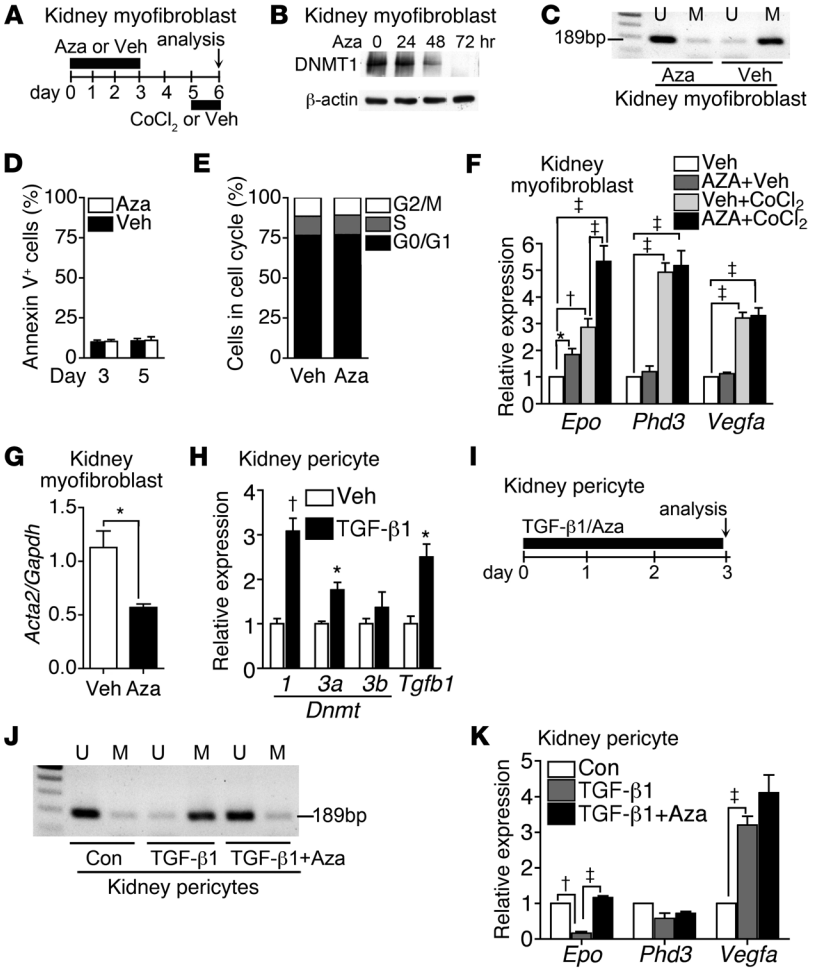

Figure 5. Aza restores EPO expression in myofibroblasts and TGF-β1–exposed pericytes. (**A**) Schema showing $CoCl_2$ stimulation of myofibroblasts after 3-day exposure to Aza or Veh and then 2-day drug withdrawal. (**B**) Western blot analysis showing the inhibitory effect of 500 nM Aza on DNMT1 expression of UUO kidney myofibroblasts. A representative blot of 4 independent experiments is shown. (**C**) *Epo* 5′-UTR methylation in myofibroblasts determined by MSP using the same method as in Figure 4, D and E. Myofibroblasts were analyzed at day 5, as described in **A**. Representative electrophoresis of 4 independent experiments is shown. (**D**) Annexin V apoptosis assay of myofibroblasts at day 3 and day 5, as described in **A**. $n = 4$ per group per time point. (**E**) Cell cycle analysis of myofibroblasts by measuring DNA content using propidium iodide staining at day 5, as described in **A**. The data were means of 4 independent experiments. (**F**) Expression of *Epo*, *Phd3*, and *Vegfa* in myofibroblasts with or without $CoCl_2$ for 16 hours. Transient exposure to Aza was performed, as described in **A**. $n = 4$ per group. (**G**) Expression of *Acta2* in myofibroblasts at day 5, as described in **A**. $n = 4$ per group. (**H**) Expression of *Dnmt1*, *Dnmt3a*, *Dnmt3b*, and *Tgfb1* in kidney pericytes cultured in medium containing 5 ng/ml TGF-β1 or Veh for 24 hours. $n = 4$ per group. (**I**) Schema illustrating the culture of pericytes with or without TGF-β1 in the presence of 500 nM Aza or Veh. (**J**) Methylation of *Epo* 5′-UTR in pericytes determined by MSP at day 3, as described in **I**. Representative electrophoresis of 4 independent experiments is shown. (**K**) Expression of *Epo*, *Phd3* and *Vegfa* in pericytes at day 3, as described in **I**. $n = 4$ per group. One-way ANOVA was used for analyses of data in **D**, **F**, **H**, and **K**, and Student's *t* test was used for analyses of data in **E** and **G**. $^*P < 0.05$, $^\dagger P < 0.01$, $^\ddagger P < 0.001$.

treated mice with Aza or PBS vehicle (Veh) after UUO surgery to study whether DNA demethylation restored *Epo* expression in fibrotic kidneys (Figure 6C). The demethylating effect of Aza on *Epo* 5′-regulatory elements of kidney myofibroblasts was confirmed (Supplemental Figure 10). Phlebotomy induced *Epo* expression in CL kidneys but failed to do so in UUO kidneys of mice treated with Veh (Figure 6, D and E). In UUO kidneys, Aza treatment increased not only the basal expression of *Epo* but also phlebotomy-induced expression (Figure 6, D and E). However, the expression of *Hif1a* and *Hif2a* was not changed by Aza treatment (Supplemental Figure 11). *Epo* expression in CL kidneys and plasma EPO concentration were not changed by Aza treatment, suggesting normally functioning CL kidneys as the major source of plasma EPO in the UUO kidney fibrosis model (Figure 6, D–F).

We next studied the effect of Aza treatment on anemia and EPO expression in the adenine-induced kidney fibrosis model (Figure 7A). Indeed, Aza treatment attenuated the decrease of hematocrit and increased renal *Epo* expression and plasma EPO concentration in adenine-induced CKD mice, without adverse effects on white cell and platelet counts in peripheral blood (Figure 7, B and C, and Supplemental Figure 12). Further analyses revealed that Aza treatment led to a greater EPO response than phlebotomy (Figure 7, B and C). In addition, Aza treatment attenuated kidney fibrosis and the elevation of plasma BUN and creatinine levels (Figure 7, D and E).

Discussion

These studies report that FOXD1$^+$ progenitor-derived, *Col1a1-GFP*$^+$PDGFRβ$^+$ kidney pericytes provide a good model for studying the molecular mechanisms underlying EPO regulation in healthy and fibrotic kidneys. Our data indicate that pericytes produce EPO through HIF2α regulation, but their EPO production capability is repressed by methylation of *Epo* 5′-regulatory elements when they differentiate into myofibroblasts during kidney fibrosis. We show compelling evidence that Aza at low nontoxic doses can restore EPO production and ameliorate anemia in mouse CKD models by targeting DNA methylation.

Our data support previous studies that demonstrated REPCs in fibrotic kidneys and their EPO production capability activated by HIF stabilizers (7, 11, 14). Although many in vitro studies have shown the association between methylation of *Epo* 5′-regulatory elements and inhibition of *Epo* expression in human cancer cell lines (17–20), our data provide the first evidence to our knowledge that methylation of *Epo* 5′-regulatory elements inhibited the baseline expression and anemic induction of *Epo* in fibrotic kidneys and myofibroblasts. Demethylation of in vitro cultured myofibroblasts and TGF-β1–exposed pericytes by Aza at a clinically relevant and nontoxic concentration increased baseline expression and hypoxic induction of *Epo*. Moreover, low-dose Aza treatment in mouse CKD models restored baseline expression and enhanced anemic induction of *Epo* in fibrotic kidneys, possibly through demeth-

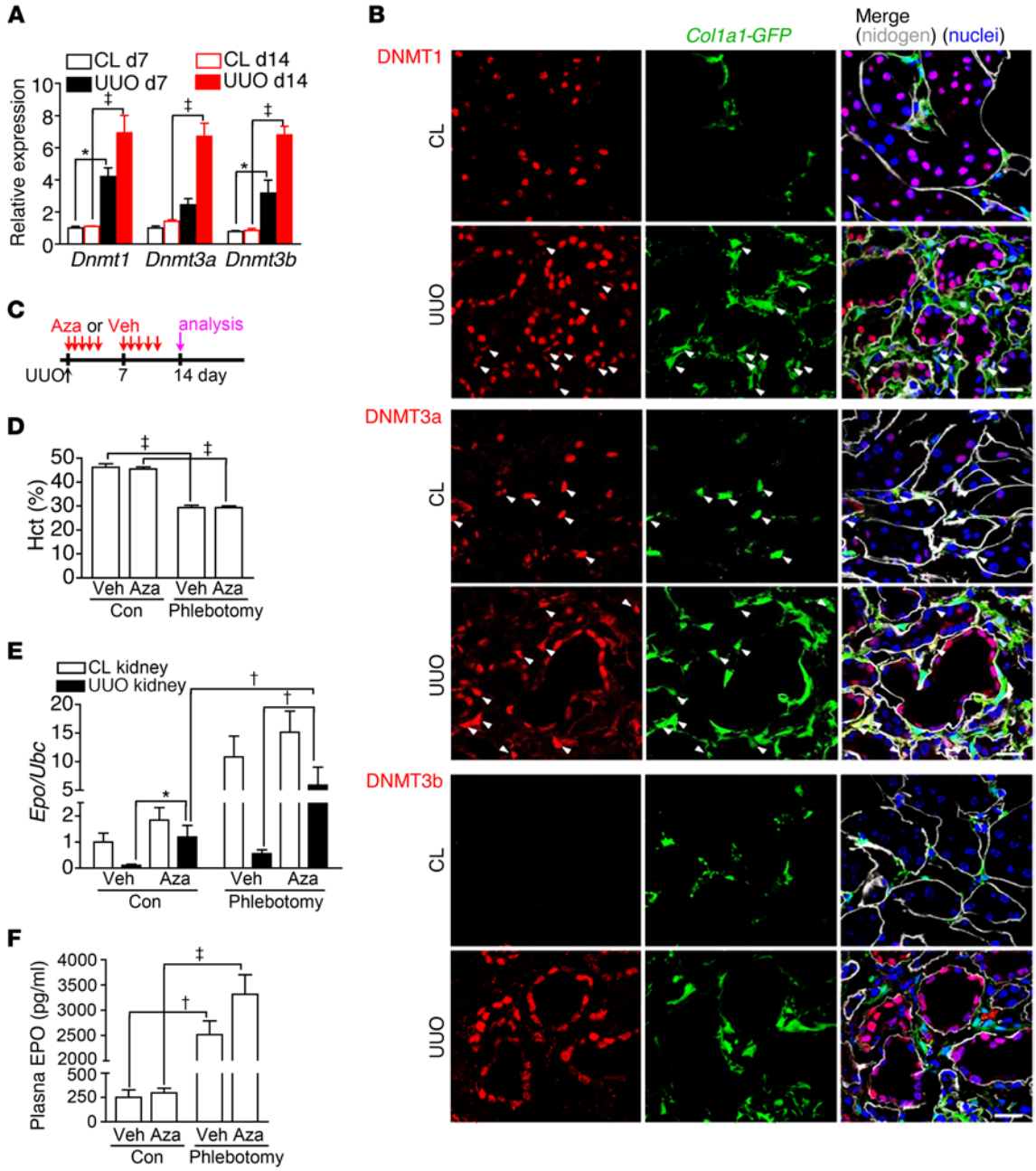

Figure 6. Aza restores EPO expression in fibrotic kidneys induced by UUO. (**A**) Expression of *Dnmt* isoforms in CL and UUO kidneys after surgery. $n = 10$ per group. (**B**) Confocal images of DNMT1, DNMT3a, DNMT3b, and nidogen staining on kidney sections of *Col1a1-GFP*^{Tg} mice. Arrowheads highlight *Col1a1-GFP*$^+$DNMT1$^+$ or *Col1a1-GFP*$^+$DNMT3a$^+$ cells. Original magnification, ×400. Scale bar: 20 μm. (**C**) Schema illustrating Aza or Veh treatment in mice after UUO surgery. Phlebotomy was or was not performed 1 day before analyses at day 14 after UUO surgery. $n = 10$ per group. (**D**–**F**) Hematocrit, renal *Epo* expression, and plasma EPO levels in mice after UUO surgery and treatment with Veh or Aza according to the schema in **C**. One-way ANOVA was used for data analyses. $^*P < 0.05$, $^\dagger P < 0.01$, $^\ddagger P < 0.001$.

ylating *Epo* 5′-regulatory elements in myofibroblasts, thereby increasing the plasma EPO concentration and ameliorating renal anemia. The potential effect of Aza on the redifferentiation of myofibroblasts into pericytes could also contribute to the restoration of *Epo* expression. In addition, our data showed that low-dose Aza treatment could prevent kidney fibrosis in mouse CKD models. The antifibrotic property of Aza could be ascribed to not only the potential effect of Aza on redifferentiating myofibroblasts back into pericytes, but also to the effect of *Rasal1* demethylation in myofibroblasts that was reported previously (32). Although *Rasal1* demethylation was shown to deactivate myofibroblasts, we are not sure whether the dose of 10 mg/kg Aza every other day in mice with folic acid nephropathy attenuated fibrosis through cytotoxic effect (32). Our own pilot experiments have shown adverse effects, including myelosuppression and body weight loss in mice after UUO surgery and in adenine-induced CKD mice treated with daily injection of Aza for 5 days per week at doses higher than or equal to 2 mg/kg and 0.5 mg/kg, respectively. Although it is not

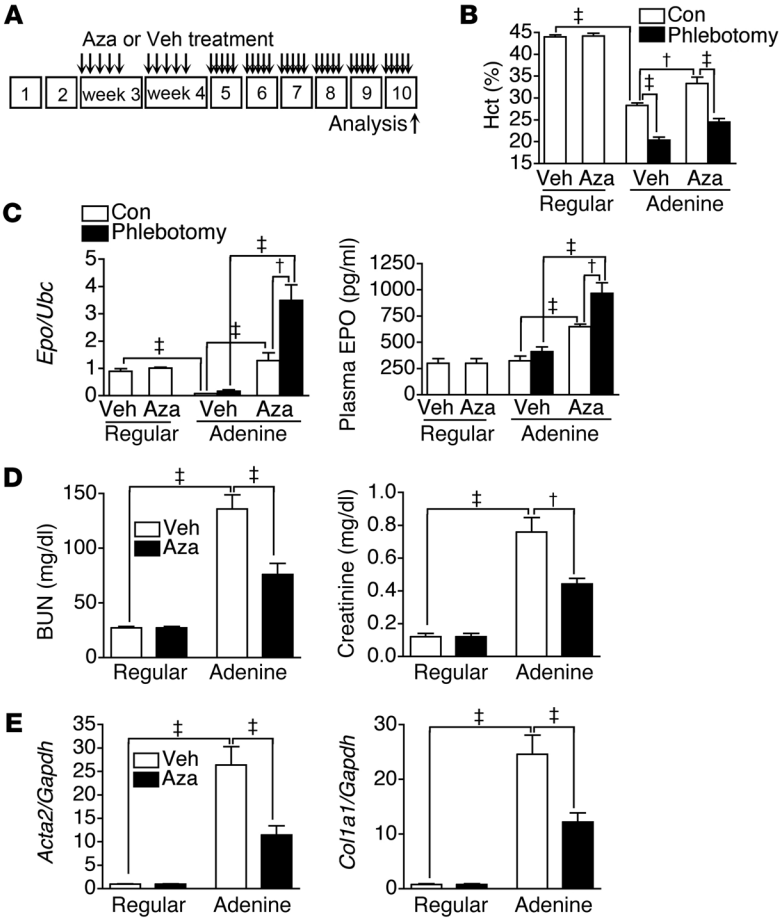

Figure 7. Aza restores EPO expression and ameliorates anemia in an adenine-induced kidney fibrosis model. (**A**) Schema illustrating Aza or Veh treatment in mice fed with regular or adenine chow, as indicated in Supplemental Figure 9A. Phlebotomy was or was not performed 1 day before analyses at week 10. n = 12 per group. (**B** and **C**) Hematocrit, renal *Epo* expression, and plasma EPO levels of mice fed with regular or adenine chow and treated with Veh or Aza according to the schema in **A**. (**D**) Plasma levels of BUN and creatinine in mice fed with regular or adenine chow and treated with Veh or Aza according to the schema in **A**. (**E**) Renal expression of *Acta2* and *Col1a1* in mice fed with regular or adenine chow and treated with Veh or Aza according to the schema in **A**. One-way ANOVA was used for data analyses. $^{\dagger}P < 0.01$, $^{\ddagger}P < 0.001$.

clear whether the high doses of Aza used in folic acid nephropathy attenuate fibrosis through cytotoxic effect (32), the low and nontoxic doses used in this study will be clinically applicable and safer for the treatment of renal fibrosis and anemia. In cancer treatment, it is emerging that low-dose demethylating agents can effectively deplete DNMTs, while high doses induce cell cycle arrest and cytotoxicity (36–38). Of the well-recognized profibrotic cytokines, we have previously shown that TGF-β1 induces pericyte-myofibroblast transition during kidney fibrosis (28–30). Here, our data further support that TGF-β1 was one of factors that led to upregulation of DNMTs and methylation and repression of *Epo* in kidney pericytes. The methylation and repression of *Epo* induced by TGF-β1 was a unique mechanism during pericyte-myofibroblast transition, because TGF-β1 affected the other HIF-regulated genes *Vegfa* and *Phd3* differently, as shown in our data.

The main reason for anemia in patients with CKD is that plasma EPO levels are unable to rise proportionately upon the decrease of hemoglobin concentration (39). Although the accumulated toxic metabolites as well as proinflammatory cytokines might inhibit the anemic induction of EPO production (11, 14, 40), intense dialysis does not restore EPO concentrations appreciably (41). Our data do not support that uremic toxins directly inhibit *Epo* expression in kidney myofibroblasts because plasma levels of BUN and creatinine are maintained within the normal range by normally functioning CL kidneys after UUO surgery. However, our data could not exclude the possibility that CL kidneys, as the major source of EPO, could inhibit *Epo* expression of UUO kidneys through produced EPO. In accordance with previous evidence (33–35), our data support the crucial role of HIF2α in *Epo* regulation of kidney pericytes. Although the PHD inhibitor can stabilize HIFs and increase plasma EPO levels in some of HD patients with atrophic kidneys (7), absolute insufficiency of HIFs should not be the reason for renal anemia, because hypoxia in the renal interstitium has been considered a hallmark of injury and mediator of CKD progression (42, 43). Our data support that methylation of *Epo* 5′-regulatory elements plays a crucial role in the disproportionate *Epo* expression in CKD by hindering the association of HIFs and the other transacting proteins with the regulatory elements (17, 18). Apparently the PHD inhibitor might attenuate the methylation-induced inhibition of *Epo* expression in kidney myofibroblasts through robust increase of HIFs for transcription initiation. However, one of the mechanisms underlying the absence of response to the PHD inhibitor in some of the patients might be hypermethylation that is too extensive to be overcome by enhanced HIFs (7). The other possible mechanism would be renal fibrosis so extensive that no viable myofibroblasts existed to produce EPO. Moreover, we should be concerned about the possible downside of long-term HIF overactivation induced by PHD inhibitor (44).

In summary, kidney pericytes produce EPO through HIF2α regulation, but this function is repressed by methylation of *Epo* 5′-regulatory elements when pericytes transit to myofibroblasts during kidney fibrosis. At low nontoxic doses, the demethylating agent Aza has produced a reversal of *Epo* repression in both kidney myofibroblasts and TGF-β1–treated kidney pericytes, leading to a rise of plasma EPO and hematocrit in CKD mice. Future studies are needed to explore the applicability of demethylating agents for renal anemia treatment in patients with CKD.

Methods

Animals. *Col1a1-GFP*^{Tg} mice, with *Col1a1*-expressing cells that expressed GFP, were generated and validated as previously described (22). B6;129S4-*Foxd1*$^{tm1(GFP/cre)Amc}$/J (referred to herein as *Foxd1*$^{Cre/+}$), *B6.Cg-Gt(ROSA)26Sor*$^{tm14(CAG-tdTomato)Hze}$*/J*, and STOCK *Epas1*^{tm1Mcs}/J (referred to herein as *Hif2a*$^{fl/fl}$) mice were obtained from The Jackson Laboratory (23, 34, 45). *Epo*$^{IRES-RFP/+}$ mice on the C57BL/6 back-

ground were generated by knocking in *IRES-RFP* between nucleotides 13432 and 13433 at *Epo* 3′-UTR of chromosome 5 (Ensembl ENSMUSG00000029711) (Supplemental Figure 1A).

Mouse models of kidney fibrosis. UUO was performed in adult (8- to 12-week-old) mice as previously described (22). Briefly, the left ureter was ligated twice using 4-0 nylon surgical sutures at the level of the lower pole of kidney. Acute adenine nephropathy was induced in adult mice fed a regular one-half inch pellet diet of LabDiet 5001 (TestDiet) containing 0.25% adenine for 21 days (Sigma-Aldrich) (46). Mice fed a regular pellet diet (LabDiet 5001) served as control. Chronic adenine nephropathy was induced in adult mice fed a regular diet with or without 0.25% adenine alternately according to the protocol shown in Supplemental Figure 9A. Analyses of hematocrit, plasma BUN, and creatinine were performed in the Laboratory Animal Center, National Taiwan University College of Medicine, Taipei, Taiwan.

Administration of Aza to mouse models of kidney fibrosis. Mice received subcutaneous daily injections of PBS Veh or Aza (0.5 mg/kg, Sigma-Aldrich) for 5 days per week after UUO surgery, as outlined in Figure 6C. Mice fed with regular or adenine chow received subcutaneous daily injections of Veh or Aza (0.125 mg/kg, reduced dose for decreased kidney function) for 5 days per week starting at week 3, as outlined in Figure 7A.

Tissue preparation and histology. Mouse tissues were prepared and stained as previously described (29). Primary antibodies against the following proteins were used for immunolabeling: αSMA-Cy3 (C6198, clone 1A4, Sigma-Aldrich), DNMT1 (5032, Cell Signaling Technology), DNMT3b (70-205, Cosmo Bio Co. LTD.), DNMT3a (sc-20703), nidogen (sc-33706, Santa Cruz Biotechnology), p75 NGF receptor (ab8875, Abcam), CD73 (550738, BD Biosciences), and PDGFRβ (a gift from William Stallcup, Burnham Institute, La Jolla, California, USA). Fluorescence-conjugated secondary antibody labeling (111-165-144, 112-165-167, 112-605-167, Jackson Immunoresearch Laboratories), DAPI staining, VECTASHIELD (Vector Laboratories) mounting, and image capture and processing were carried out as previously described (29). Quantification of specific cells in tissue sections was carried out as follows. In brief, sections were colabeled with DAPI. *Col1a1-GFP*$^+$ and EPO-RFP$^+$ cells were identified by DAPI$^+$ (blue), green, and red colocalization, respectively. αSMA$^+$ cells were identified by the presence of greater than 75% of the cell area immediately surrounding nuclei (detected by DAPI) staining positive with Cy3 fluorescence, which is indicative of antigen expression. Specific cells were counted in 10 randomly selected cortical interstitial fields at ×400 magnification (high-powered field) per mouse. Interstitial fibrosis was quantified in Picrosirius red–stained paraffin sections.

Isolation and culture of kidney pericytes and myofibroblasts. Pericytes and myofibroblasts were isolated from normal and day 14 UUO kidneys, respectively, as described previously (29). In brief, kidney was diced and incubated at 37°C for 45 minutes with Liberase (0.5 mg/ml, Roche Applied Science) and DNase (100 U/ml, Roche Applied Science) in HBSS. After centrifugation, cells were resuspended in 5 ml PBS/1% BSA and filtered (40 μm). Pericytes and myofibroblasts were isolated by sorting GFP$^+$PDGFRβ$^+$CD31$^-$E-cadherin$^-$ cells using a FACSAria cell sorter (BD Biosciences) and cultured in DMEM with 10% FBS. The percentages of pericytes and myofibroblasts of the total kidney cells gated in FACS plots isolated from normal and day 14 UUO kidneys were 0.7% ± 0.3% and 12.9% ± 0.8%, respectively. Passage 0 cells were used for experiments. In hypoxia experiments, cells were washed with 1× PBS (pH 7.4) and renewed culture medium and then placed in an incubator with 21% O_2 or in a hypoxia chamber (INVIVO2 200, Ruskinn Technology Ltd.) with 0.5% O_2 for 48 hours. Cellular RNA was harvested by adding the RLT buffer provided in the RNeasy Mini Kit (Qiagen) immediately after cells were taken out of the incubator and the supernatant was removed for storage. In $CoCl_2$ (Sigma-Aldrich) or IOX2 (Tocris Bioscience) experiments, cells were washed with 1× PBS and renewed culture medium and with or without $CoCl_2$ or IOX2. Cellular RNA was harvested at indicated time points. In TGF-β1 stimulation experiments, cells were washed with 1× PBS and renewed culture medium and with or without 5 ng/ml TGF-β1 (R&D Systems) in the presence of 500 ng/ml Aza (Sigma-Aldrich) or Veh. Cellular RNA and genomic DNA were harvested at indicated time points. In myofibroblast culture, cells were treated with 500 ng/ml Aza for 3 days and then harvested for Western blot analysis of DNMT1 or treated with $CoCl_2$ or Veh after a 2-day Aza-free period. Cellular RNA was then harvested after $CoCl_2$ or Veh treatment.

PCR. Total RNA was extracted using the RNeasy Mini Kit (Qiagen). The purity of each sample was determined based on the ratio of A260 to A280. cDNA was synthesized using the iScript cDNA Synthesis Kit (Bio-Rad). Genomic DNA was extracted using the DNeasy Blood & Tissue Kit (Qiagen). Conventional and quantitative PCR were performed using methods described previously (28). Expression levels were normalized by ubiquitin C (*Ubc*) or *Gapdh*. The specific primer pairs used for PCR are listed in Supplemental Tables 1 and 2.

COBRA. Genomic DNA was prepared from *Col1a1-GFP*$^+$PDGFRβ$^+$CD31$^-$E-cadherin$^-$ pericytes and myofibroblasts isolated from normal kidneys and kidneys 14 days after UUO surgery of *Col1a1-GFP*^{Tg} mice, respectively. Sodium bisulfite conversion of genomic DNA was performed using the EZ DNA Methylation Kit according to the manufacturer's protocol (ZYMO Research). PCR using bisulfite-converted genomic DNA as the template and the primers shown in Supplemental Table 2 would amplify the genomic DNA fragments containing promoter and 5′-UTR of *Epo*. Unmethylated and methylated controls were from mouse sperm genomic DNA and Methylated Mouse Genomic DNA Standard, respectively (ZYMO Research). Equal amount of the PCR products were incubated in buffer with or without restriction enzyme BstUI at 60°C for 3 hours (New England Biolabs), and then electrophoresis was performed in a 1% agarose gel.

BGS. Genomic DNA was prepared and sodium bisulfite conversion of genomic DNA was performed as described for those in *COBRA*. PCR products of the genomic DNA fragment containing promoter and 5′-UTR or distal 5′-enhancer amplified from bisulfite-converted genomic DNA using the primers shown in Supplemental Table 2 were gel purified with the QIAquick Gel Extraction Kit (QIAGEN). The eluted DNA fragments were ligated into pGEM-T Easy Vector (Promega Corporation) for sequencing. Four colonies for each mouse were randomly chosen for sequencing.

MSP. Genomic DNA was prepared and sodium bisulfite conversion of genomic DNA was performed as described for those in *COBRA*. Bisulfite-converted genomic DNA was amplified with methylation-specific or unmethylation-specific primer pairs shown in Supplemental Table 3. Unmethylated and methylated controls were from mouse sperm genomic DNA and Methylated Mouse Genomic DNA Standard, respectively (ZYMO Research). The PCR products were analyzed by electrophoresis. The electrophoresis result was shown as a virtual gel. The percentage of methylation of

Epo 5′-UTR for the indicated cells was determined by densitometric analysis of MSP products (methylated products divided by the sum of methylated and unmethylated products).

Western blot analysis. Total cellular protein extracted using RIPA buffer was subjected to Western blot analysis using methods described previously (28). The following primary antibodies were used to detect protein: DNMT1 (5032, Cell Signaling Technology) and β-actin (4967, Cell Signaling Technology).

Detection of EPO in plasma and culture media. Mouse heparin plasma and pericyte culture supernatant stored in a –80°C freezer after collection were transferred into a –20°C freezer 12 to 16 hours prior to analysis and thawed on ice before analysis. The analysis was performed according to the protocol of provided in the Mouse Erythropoietin Quantikine ELISA Kit (R&D Systems).

Statistics. Data are expressed as mean ± SEM. Statistical analyses were carried out using GraphPad Prism (GraphPad Software). Statistical significance was evaluated by Student's *t* tests or 1-way ANOVA. *P* values of less than 0.05 were considered significant.

Study approval. All animal studies were carried out under a protocol approved by the Institutional Animal Care and Use Committee of the National Taiwan University College of Medicine.

Author contributions

YTC, CCY, SYP, YHC, FCC, CFL, MHT, and HLH carried out experiments and analyzed data. CHL, WCC, MSW, TSC, and YMC participated in experiment design and data analysis. YMC and SLL designed and directed the project, carried out experiments, analyzed data, and wrote the manuscript.

Acknowledgments

We thank David Brenner (UCSD, La Jolla, California, USA) and Jeremy Duffield (University of Washington, Seattle, Washington, USA) for *Col1a1-GFP*^{Tg} mice; William Stallcup (Burnham Institute, La Jolla, California, USA) for anti-PDGFRβ antibody; the Core Laboratories of the Department of Medical Research of National Taiwan University Hospital; the Cell Sorting Core Facility and Imaging Core Facility of the First Core Laboratory of National Taiwan University College of Medicine for equipment support and technical assistance; the Transgenic Mouse Model Core Facility of the National Core Facility Program for Biotechnology, the Ministry of Science and Technology (MOST), Taiwan; the Gene Knockout Mouse Core Laboratory of National Taiwan University Center of Genomic Medicine; and Mars T.Y. Lin for editing the manuscript. Y.M. Chen is supported by MOST (101-2314-B-002-084, 104-2314-B-002-156). S.L. Lin is supported by MOST (102-2628-B-002-015, 102-2321-B002-045, 103-2321-B-002-014), National Taiwan University Hospital (102-S2042, 103-S2405, 104-UN015, 104-EDN02), National Taiwan University (NTU-ICRP-104R7559-2), and the Mrs. Hsiu-Chin Lee Kidney Research Foundation.

Address correspondence to: Shuei-Liong Lin, Graduate Institute of Physiology, No. 1, Jen-Ai Road Section 1, Taipei, Taiwan 100. Phone: 886.2.23123456, ext. 88235; E-mail: linsl@ntu.edu.tw. Or to: Yung-Ming Chen, Department of Internal Medicine, No. 7, Chung-Shan South Road, Taipei, Taiwan 100. Phone: 886.2.23123456, ext. 65993; E-mail: chenym@ntuh.gov.tw.

1. Erslev AJ. Erythropoietin. *N Engl J Med*. 1991;324(19):1339–1344.
2. Eschbach JW. Erythropoietin 1991 — an overview. *Am J Kidney Dis*. 1991;18(4 suppl 1):3–9.
3. Brookhart MA, et al. The effect of altitude on dosing and response to erythropoietin in ESRD. *J Am Soc Nephrol*. 2008;19(7):1389–1395.
4. Walle AJ, Wong GY, Clemons GK, Garcia JF, Niedermayer W. Erythropoietin-hematocrit feedback circuit in the anemia of end-stage renal disease. *Kidney Int*. 1987;31(5):1205–1209.
5. Chandra M, Clemons GK, McVicar MI. Relation of serum erythropoietin levels to renal excretory function: evidence for lowered set point for erythropoietin production in chronic renal failure. *J Pediatr*. 1988;113(6):1015–1021.
6. Erslev AJ, Caro J, Kansu E, Silver R. Renal and extrarenal erythropoietin production in anaemic rats. *Br J Haematol*. 1980;45(1):65–72.
7. Bernhardt WM, et al. Inhibition of prolyl hydroxylases increases erythropoietin production in ESRD. *J Am Soc Nephrol*. 2010;21(12):2151–2156.
8. Maxwell PH, et al. Identification of the renal erythropoietin-producing cells using transgenic mice. *Kidney Int*. 1993;44(5):1149–1162.
9. Bachmann S, Le Hir M, Eckardt KU. Co-localization of erythropoietin mRNA and ecto-5′-nucleotidase immunoreactivity in peritubular cells of rat renal cortex indicates that fibroblasts produce erythropoietin. *J Histochem Cytochem*. 1993;41(3):335–341.
10. Obara N, Suzuki N, Kim K, Nagasawa T, Imagawa S, Yamamoto M. Repression via the GATA box is essential for tissue-specific erythropoietin gene expression. *Blood*. 2008;111(10):5223–5232.
11. Asada N, et al. Dysfunction of fibroblasts of extrarenal origin underlies renal fibrosis and renal anemia in mice. *J Clin Invest*. 2011;121(10):3981–3990.
12. Bussolati B, Lauritano C, Moggio A, Collino F, Mazzone M, Camussi G. Renal CD133(+)/CD73(+) progenitors produce erythropoietin under hypoxia and prolyl hydroxylase inhibition. *J Am Soc Nephrol*. 2013;24(8):1234–1241.
13. Yamazaki S, et al. A mouse model of adult-onset anaemia due to erythropoietin deficiency. *Nat Commun*. 2013;4:1950.
14. Souma T, et al. Plasticity of renal erythropoietin-producing cells governs fibrosis. *J Am Soc Nephrol*. 2013;24(10):1599–1616.
15. Suzuki N, et al. Specific contribution of the erythropoietin gene 3′ enhancer to hepatic erythropoiesis after late embryonic stages. *Mol Cell Biol*. 2011;31(18):3896–3905.
16. Storti F, et al. A novel distal upstream hypoxia response element regulating oxygen-dependent erythropoietin gene expression. *Haematologica*. 2014;99(4):e45–e48.
17. Yin H, Blanchard KL. DNA methylation represses the expression of the human erythropoietin gene by two different mechanisms. *Blood*. 2000;95(1):111–119.
18. Dewi FR, Fatchiyah F. Methylation impact analysis of erythropoietin (EPO) gene to hypoxia inducible factor-1alpha (HIF-1α) activity. *Bioinformation*. 2013;9(15):782–787.
19. Rossler J, et al. Hypoxia-induced erythropoietin expression in human neuroblastoma requires a methylation free HIF-1 binding site. *J Cell Biochem*. 2004;93(1):153–161.
20. Steinmann K, Richter AM, Dammann RH. Epigenetic silencing of erythropoietin in human cancers. *Genes Cancer*. 2011;2(1):65–73.
21. Duffield JS. Cellular and molecular mechanisms in kidney fibrosis. *J Clin Invest*. 2014;124(6):2299–2306.
22. Lin SL, Kisseleva T, Brenner DA, Duffield JS. Pericytes and perivascular fibroblasts are the primary source of collagen-producing cells in obstructive fibrosis of the kidney. *Am J Pathol*. 2008;173(6):1617–1627.
23. Humphreys BD, et al. Fate tracing reveals the pericyte and not epithelial origin of myofibroblasts in kidney fibrosis. *Am J Pathol*. 2010;176(1):85–97.
24. Lin SL, et al. Targeting endothelium-pericyte crosstalk by inhibiting VEGF receptor signaling attenuates kidney microvascular rarefaction and fibrosis. *Am J Pathol*. 2011;178(2):911–923.
25. Schrimpf C, et al. Pericyte TIMP3 and ADAMTS1 modulate vascular stability after kidney injury. *J Am Soc Nephrol*. 2012;23(5):868–883.
26. Chang FC, Chou YH, Chen YT, Lin SL. Novel insights into pericyte-myofibroblast transition and therapeutic targets in renal fibrosis. *J Formos Med Assoc*. 2012;111(11):589–598.

27. Kramann R, et al. Perivascular Gli1+ progenitors are key contributors to injury-induced organ fibrosis. *Cell Stem Cell*. 2015;16(1):51–66.
28. Chen YT, et al. Platelet-derived growth factor receptor signaling activates pericyte-myofibroblast transition in obstructive and post-ischemic kidney fibrosis. *Kidney Int*. 2011;80(11):1170–1181.
29. Wu CF, et al. Transforming growth factor beta-1 stimulates profibrotic epithelial signaling to activate pericyte-myofibroblast transition in obstructive kidney fibrosis. *Am J Pathol*. 2013;182(1):118–131.
30. Ren S, et al. LRP-6 is a coreceptor for multiple fibrogenic signaling pathways in pericytes and myofibroblasts that are inhibited by DKK-1. *Proc Natl Acad Sci U S A*. 2013;110(4):1440–1445.
31. Castano AP, et al. Serum amyloid P inhibits fibrosis through FcγR-dependent monocyte-macrophage regulation in vivo. *Sci Transl Med*. 2009;1(5):5ra13.
32. Bechtel W, et al. Methylation determines fibroblast activation and fibrogenesis in the kidney. *Nat Med*. 2010;16(5):544–550.
33. Gruber M, Hu CJ, Johnson RS, Brown EJ, Keith B, Simon MC. Acute postnatal ablation of Hif-2α results in anemia. *Proc Natl Acad Sci U S A*. 2007;104(7):2301–2306.
34. Kapitsinou PP, et al. Hepatic HIF-2 regulates erythropoietic responses to hypoxia in renal anemia. *Blood*. 2010;116(16):3039–3048.
35. Paliege A, et al. Hypoxia-inducible factor-2α-expressing interstitial fibroblasts are the only renal cells that express erythropoietin under hypoxia-inducible factor stabilization. *Kidney Int*. 2010;77(4):312–318.
36. Tsai H-C, et al. Transient low doses of DNA-demethylating agents exert durable antitumor effects on hematological and epithelial tumor cells. *Cancer Cell*. 2012;21(3):430–446.
37. Shen H, Laird PW. In epigenetic therapy, less is more. *Cell Stem Cell*. 2012;10(4):353–354.
38. Issa J-PJ, et al. Phase 1 study of low-dose prolonged exposure schedules of the hypomethylating agent 5-aza-2′-deoxycytidine (decitabine) in hematopoietic malignancies. *Blood*. 2004;103(5):1635–1640.
39. Erslev AJ, Besarab A. Erythropoietin in the pathogenesis and treatment of the anemia of chronic renal failure. *Kidney Int*. 1997;51(3):622–630.
40. Chiang CK, Tanaka T, Inagi R, Fujita T, Nangaku M. Indoxyl sulfate, a representative uremic toxin, suppresses erythropoietin production in a HIF-dependent manner. *Lab Invest*. 2011;91(11):1564–1571.
41. Radtke HW, Frei U, Erbes PM, Schoeppe W, Koch KM. Improving anemia by hemodialysis: effect of serum erythropoietin. *Kidney Int*. 1980;17(3):382–387.
42. Tanaka T, Nangaku M. The role of hypoxia, increased oxygen consumption, and hypoxia-inducible factor-1 α in progression of chronic kidney disease. *Curr Opin Nephrol Hypertens*. 2010;19(1):43–50.
43. Wang Z, et al. Hypoxia-inducible factor-1α contributes to the profibrotic action of angiotensin II in renal medullary interstitial cells. *Kidney Int*. 2011;79(3):300–310.
44. Pritchett TL, Bader HL, Henderson J, Hsu T. Conditional inactivation of the mouse von Hippel-Lindau tumor suppressor gene results in wide-spread hyperplastic, inflammatory and fibrotic lesions in the kidney. *Oncogene*. 2015;34(20):2631–2639.
45. Chen YT, et al. Lineage tracing reveals distinctive fates for mesothelial cells and submesothelial fibroblasts during peritoneal injury. *J Am Soc Nephrol*. 2014;25(12):2847–2858.
46. Tamura M, Aizawa R, Hori M, Ozaki H. Progressive renal dysfunction and macrophage infiltration in interstitial fibrosis in an adenine-induced tubulointerstitial nephritis mouse model. *Histochem Cell Biol*. 2009;131(4):483–490.